Smartphone-Based Interrogation of a Chirped FBG Strain Sensor Inscribed in a Multimode Fiber

Aleksandr A. Markvart, Leonid B. Liokumovich, Iurii O. Medvedev, and Nikolai A. Ushakov

***Abstract*—Smartphone-based interrogation of a fiber Bragg grating sensor is, to the best of our knowledge, reported for the first time. The smartphone flashlight LED was used as a light source and a transmissive diffraction grating projected the CFBG spectra on the smartphone camera. In order to efficiently couple light from the smartphone LED to the fiber with CFBG, multimode fiber was used for inscription. Interrogation setup consists of a smartphone and low-cost off-the-shelf available components. Measurement principle was illustrated through the fiber strain caused by applied longitudinal force. Attained measurement sensitivity and resolution were validated via comparison with commercial spectrometer and theoretical results based on Cramer–Rao approach. Also, to the best of our knowledge, the influence of modal noise on the smartphone-based fiber optic sensor interrogation system performance is considered for the first time.**

***Index Terms*—Chirped fiber bragg grating, cramer-rao bound, fiber bragg grating, modal noise, multimode optical fiber sensor, smartphone-based optical spectrometer, smartphone-based sensor.**

I. Introduction

OPTICAL fiber sensors (OFS) are a prominent research area, which draws significant attention from scientific groups all over the world. Thousands of companies develop commercially available OFS systems. OFS applications span from oil&gas, avionics and seismic to health care and biology, internet of things (IoT) and many others [1]–[5]. The advantages of OFS include high sensitivities and resolutions, immunity to electromagnetic interference, ability to multiplex several sensing elements, small footprint, chemical neutrality, ability to operate in harsh environments. One of the most popular and commercially successful type of optical fiber sensors is based on fiber Bragg gratings [6] created by periodically modulating the refractive index in a short section of an optical fiber core. Reflective spectrum of FBG appears to be a narrow sharp peak [7], which shifts if a certain perturbation affects the FBG. One of the most widely used techniques to measure the shift of the FBG spectrum involves an optical source with wide spectrum and an optical spectrum analyzer [8], which enables one to directly observe the spectral shift.

Due to rapid development of smartphones and other portable gadgets, there is a strong interest in applying them for interrogation of optical sensors [9]–[12], including fiber optic ones [1], [13]–[18]. Further development of such techniques will pave the way for low-cost, widespread and easily reconfigurable optical fiber sensing systems, easily integrated with existent telecommunication infrastructure. An increase in computing capabilities of smartphones and bandwidth of wireless communication protocols will allow to create distributed sensing meshes for various tasks, ranging from structure health monitoring to biomedical inspection. Even though some steps towards the FBG interrogation with portable devices have been made [19], it's the smartphones' LED flashlights that impose a fundamental limitation on the use of conventional optical fiber sensors with smartphones. It is due to the fact that LEDs irradiate spatially incoherent light, which can't be efficiently coupled to a single-mode fiber [20]–[22]. Therefore, only multimode fibers can be used with fully smartphone-based interrogation systems (not incorporating any external devices, such as light source). However, a possibility for developing smartphone-based FBG interrogation systems is created thanks to the recent progress in techniques for FBG inscription into multimode fibers [23], especially into polymer fibers [24], [25], which demonstrate outstanding strain sensitivities.

In this work a smartphone-based FBG sensor interrogation system is, to the best of our knowledge, reported for the first time. The sensor is a chirped fiber Bragg grating (CFBG) inscribed in a graded-index multimode fiber (MM). This allowed to efficiently couple the smartphone LED to the fiber containing the sensor. The interrogation setup consists of low-cost and readily available components: a smartphone, a piece of a DVD disk, a razor blade slit and a 3D-printed holder.

II. Smartphone-Based CFBG Interrogation Prototype

The concept of the smartphone-based interrogation system, similar to most of the already known smartphone-based spectrometers (SPBS) [12], [13], [16] is depicted in Fig. 1(a). The smartphone LED was used as a light source. SPBS was assembled using the smartphone camera, a piece of a DVD disk acting as a diffraction grating and a slit consisting of two halves of a razor blade. These components were fixed on a 3D-printed

Manuscript received May 30, 2020; revised August 14, 2020; accepted September 12, 2020. Date of publication September 18, 2020; date of current version January 2, 2021. This research work was supported by the Academic Excellence Project 5-100 proposed by Peter the Great St. Petersburg Polytechnic University, Project # 4.2.1.2. *(Corresponding author: Aleksandr Markvart.)*

Aleksandr A. Markvart, Leonid B. Liokumovich, and Nikolai A. Ushakov are with the Institute of Physics, Nanotechnology, and Telecommunications, Peter the Great St. Petersburg Polytechnic University, 195251 St. Petersburg, Russia (e-mail: markvart_aa@spbstu.ru; leonid@spbstu.ru; n.ushakoff@spbstu.ru).

Iurii O. Medvedev is with the Institute of Systems and Robotics, University of Coimbra, Rua Silvio Lima - Polo II, 3030-290 Coimbra, Portugal (e-mail: iurii.medvedev@isr.uc.pt).

Color versions of one or more of the figures in this article are available online at https://ieeexplore.ieee.org.

Digital Object Identifier 10.1109/JLT.2020.3024713

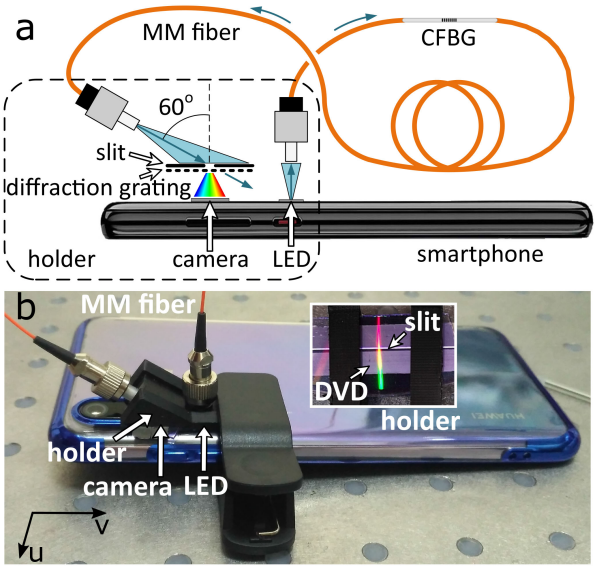

Fig. 1. The schematic overview (a) and the photograph (b) of the developed smartphone-based CFBG interrogation system. The inset in the photo demonstrates a DVD-based grating and a razor blade slit combined on the 3D-printed holder. Physical representation of the u and v coordinates of the spectrum image is shown in the bottom-left corner of the figure.

holder, attached to the smartphone with a peg. The interrogated CFBG was inscribed in the multimode fiber which was coupled to the smartphone LED and the spectrometer through the above-mentioned 3D-printed holder. The photo of the assembled system is shown in Fig. 1(b), the inset shows the part of the setup, containing a piece of a DVD disk and a razor blade slit.

In this study we have used graded index multimode fiber (G.651) with a core diameter of 50 μm and numeric aperture 0.22. A 15 mm-long chirped fiber Bragg grating (CFBG) has been inscribed with a KrF excimer laser system and a Talbot interferometer. The inscription system is described in detail in [26]. The reference transmission spectra of the grating were measured with a LED and a Hamamatsu C10082CAH spectrometer, which spectral resolution (defined as a full width at half maximum (FWHM) of an ISRF) is $\delta\lambda = 1$ nm and wavelength sampling interval at 634 nm is $\Delta = 0.35$ nm/pixel. A spectrum example is shown in Fig. 2(a). FWHM of the measured CFBG spectrum is $\sim$6 nm with peak reflectivity of 18% at 634 nm.

The CFBG was used as a sensitive element in order to avoid the multi-peak behaviour of fiber grating spectra typically observed in multimode fibers [27] due to the mode dispersion. In turn, spectrum of a CFBG is a superposition of broadened peaks corresponding to individual mode groups, resulting in a broadened but nevertheless single peak, shown in Fig. 2(a). This effect was enhanced thanks to limited spectral resolution of the spectrometer. CFBG inscription in a limited area of fiber cross-section [28] is another way of obtaining a single-peak spectrum of a fiber grating inscribed in MM fiber, however, such gratings interact only with the fundamental mode, leaving the rest of the modes unaltered. Therefore, the visibility of the dip in the transmission spectrum will be negligible, sufficiently degrading the sensor resolution.

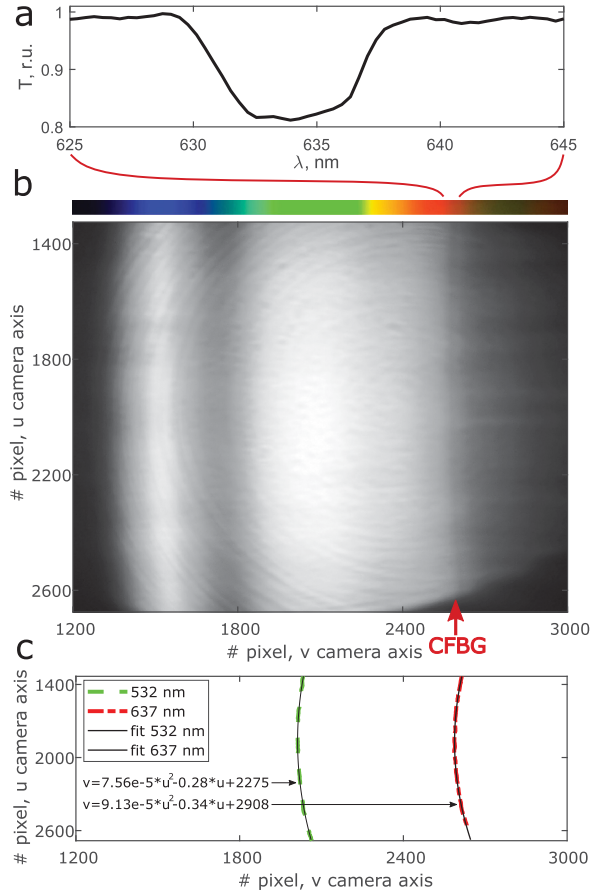

Fig. 2. Spectra of the CFBG obtained with (a) commercial spectrometer and (b) smartphone-based spectrometer. (c) Wavelength calibration of the SPBS using two laser pointers (emission peaks at $\lambda_{green} \approx 532$ nm and $\lambda_{red} \approx 637$ nm).

In order to detect subnanometer shifts of a Bragg wavelength (BW), we have used a smartphone with a high-performance camera, namely, Huawei P20 PRO model. It has a 20 megapixels, 1/2.78" monochrome sensor with f/1.6-aperture lens produced by Leica. The use of the monochrome sensor has advantages in comparison with RGB sensors such as higher resolution and several times higher signal-to-noise ratio (SNR).

A transparent piece of a DVD+R disk has been used as a low-cost and readily available diffraction grating. Its spiral guide groove has a sufficiently fine and regular pitch of 0.74 μm, which allows to use the DVD as a transmission diffraction grating. The entrance slit has been mounted on the top of the DVD piece. On the one hand, the performance of the diffraction grating is optimal in case of an incident plane wave [29] (which is equivalent to parallel rays in geometric optics approximation). However, the beam exiting the multimode fiber with numeric aperture 0.22 has a large divergence angle about 25 degrees. Therefore, the slit extracts a relatively small portion of the wave front (containing rays within reduced angular range) exiting the fiber, which determines the spectral resolution of the spectrometer. On the other hand, the broader is the beam incident on the diffraction grating (the wider is the slit), the higher signal intensity can be achieved. The slit width of 70 μm was set to

achieve a trade-off between the spectrometer resolution and the signal quality.

A custom-made holder has been 3D-printed from ABS plastic. It performs two functions: 1) it combines the DVD diffraction grating and the slit; 2) it holds the first FC-PC connector for coupling the LED light to the fiber, and the second FC-PC connector tilted at a 60^0 angle with respect to the vertical axis for coupling the light exiting the fiber to the SPBS. In case of 60^0 angle, the 1st-order diffraction beam falls to the camera sensor while the 0-order beam does not.

In order to perform the measurements the smartphone LED and the camera were turned on. The camera was switched to the manual mode for precise settings adjustment. As the light beam irradiated from the fiber end is subject to diffraction-caused divergence, the camera focus was set to minimal value in order to obtain a sharper spectrum image with minimal distortions. In order to obtain maximal SNR the ISO was set to minimal value of 50, while the exposure time was adjusted to 1.6 s, in which case the signal spanned the whole 8-bit scale of the camera sensor without any saturation.

The photo of the CFBG transmission spectra is presented in Fig. 2(b). In such a way, rows of the presented 2-dimensional spectrum (along the v axis) correspond to individual spectra realizations, denoted as raw one-dimensional spectra (R1DS), and the whole image must be averaged along the u axis in order to obtain a single spectrum. It can be seen that there is an indistinct black radial curve on the right-hand side of the photo which corresponds to the Bragg transmission dip (it is marked with a CFBG sign and an arrow). However, it should be noted that since the groves in the DVD disk are radial, the curve corresponding to CFBG dip is also radial. Therefore, prior to image averaging, the R1DS must be shifted in such a manner that the CFBG dip position coincides in all of them, which can be easily performed after the wavelength scales for all R1DS are calibrated.

III. Sensor Calibration and Signal Processing

In order to calibrate the wavelength scale of the assembled SPBS, we have used two laser pointers with 532 nm and 637 nm wavelengths, respectively, which were connected to SPBS via a conventional graded-index MM 50 μm patchcord. The response to each laser in registered 2D spectrum would be a 2D sickle-like figure, which cross-sections along the v axis are very narrow and are shifted with respect to their positions along the u axis. The positions of the peaks corresponding to different lasers would provide information about the wavelength scale of the SPBS. Obviously, speckles, caused by intermode interference of coherent light [30], [31] at the output of MM fiber, were observed in the registered 2D spectra. In order to eliminate speckle influence on the calibration results, spectra were registered several times, while the patchcord was bent and re-shaped, which caused the change of the intermode phase relations, and hence, the speckle pattern [31]. The obtained spectra were averaged, resulting in a significant decrease in speckle visibility.

In the resultant averaged 2D spectra each dependence of R1DS on v coordinate was fitted by a gaussian function, hence, giving the maximum positions used to align the CFBG spectra.

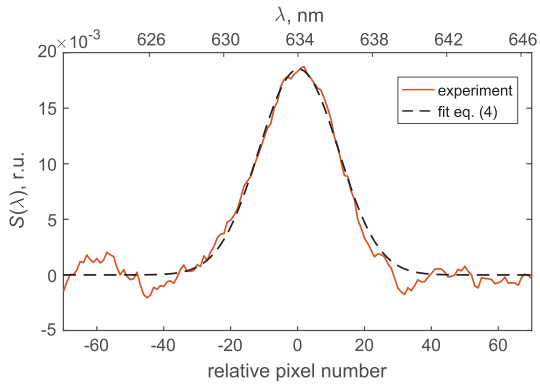

Fig. 3. Example of inverted CFBG spectrum and its gaussian fit according to eq. (1).

The calculated positions vs. the pixel number along the u axis are depicted in Fig. 2(c). The dependencies of maximum positions on the u pixel number were approximated by second-order polynomials, which were subsequently used for the wavelength scale calculation and the rows alignment. The equations describing the fits are shown in Fig. 2(c). Although the coefficients of the fitting equations are slightly different, the actual difference between the wavelength scales of different R1DS was less than 1%. The difference between the positions of spectra corresponding to 532 nm and 637 nm lasers was used to calculate the sampling interval of the wavelength scale of assembled SPBS which turned out to be $\Delta = 0.18$ nm per pixel.

After performing the rows alignment, the shifted R1DS were averaged along the u axis over all the rows containing CFBG transmission dips. Then, the resultant spectra were normalized on the illuminating LED's spectra shape, which, in turn, was measured in the same manner with rows alignment and averaging. However, the fiber with CFBG was replaced by a conventional graded index MMF patchcord.

Examples of processed CFBG spectra are presented in Figs. 3 and 4(a). Compared with the spectrum obtained by commercial Hamamatsu spectrometer, shown in Fig. 2(a); the FWHM of the CFBG spectra measured with SPBS turns out to be around 6 nm, which is the same as the one measured with Hamamatsu spectrometer, indicating that the spectral resolution $\delta\lambda$ of the assembled SPBS is close to 1 nm. Different amplitudes of CFBG dips are likely to be caused by non-uniform distribution of refractive index modulation across the fiber cross-section and hence, unequal interaction of different fiber modes with the grating. In turn, different slit widths of the used spectrometers resulted in different spatial filtering of incoming light. Namely, narrower slit width in Hamamatsu spectrometer prevented higher-order modes that didn't interact with the CFBG from being captured by the spectrometer. On the other hand, wider slit in the SPBS resulted in higher number of modes being measured, however, since they were not spectrally filtered by the CFBG, they contributed only to the constant component of the spectrum, thus decreasing the visibility of the measured CFBG spectrum. The spatial nonuniformity of the inscribed CFBG is the drawback of using the inscription setup that was suited to work with single-mode fibers and potentially can be overcame by the use of

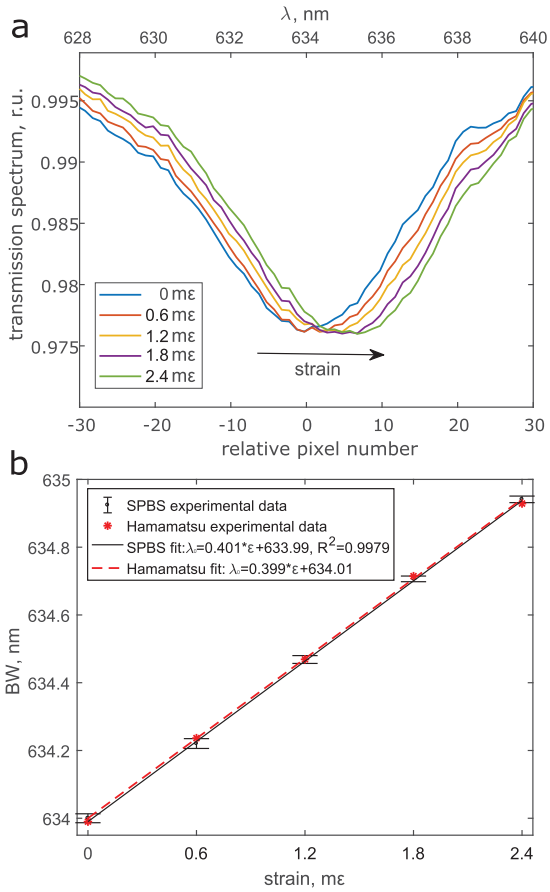

Fig. 4. Strain sensitivity of developed sensing system: spectra shift due to applied strain (a), relation of the measured BW with applied strain for two experimental setup: SPBS and Hamamatsu spectrometer (b).

point-by-point inscription technique [32]. This and also different shapes of the ISRF of SPBS and Hamamatsu spectrometer attributes to different shapes of the measured spectra.

After obtaining the CFBG spectrum, it could be processed in order to find the Bragg wavelength, which value represents the quantity to be measured. One of the most straightforward and accurate ways to demodulate the BW is to fit the measured spectrum with an analytical function. Since FBG spectrum (and CFBG especially) is described by a relatively complex function containing several grating parameters [7] that are not directly relevant to the measurement process, a simpler fitting model such as Gaussian is typically applied [33], [34]. Therefore, the BW can be found by fitting the CFBG spectrum by equation

$$S_i(\lambda_0, w, A) = A \exp(-(\lambda_i - \lambda_0)^2/(2\,w^2)), \qquad (1)$$

where S_i is the i-th spectral point of the gaussian function, A is the amplitude of the gaussian peak, λ_i is the i-th wavelength point, λ_0 is the position of the center of the peak or Bragg wavelength, w is the half width at $1/\sqrt{e}$ of maximum. The three parameters A, w and λ_0 are found as a result of fitting procedure. An example of experimentally measured CFBG spectrum and its gaussian fit is shown in Fig. 3, R^2 value of the fit was 0.98. Therefore, the model in eq. (1) is in a very good agreement with the shape of the experimental spectrum and can be used for BW demodulation.

The signal processing was performed in MATLAB Mobile app, installed on the smartphone. MATLAB Mobile is a lightweight desktop on a smartphone that connects to a MATLAB session running on the MathWorks Computing Cloud.

We have also tested the temperature stability of the assembled smartphone-based measurement system. For that, the SPBS was placed in an environmentally-isolated box, conditions in which could be controlled by an intrinsic heater. The same 637 nm laser was used as a light source, for which the ambient conditions were constant. The position of the laser spectrum was monitored as described above, and was recorded during the temperature change inside the chamber. The temperature was varied from 15 Celsius to 45 Celsius with a 10 degree step, the spectrum position shift was proportional to the temperature with overall shift 0.72 nm, resulting in $\sim$24pm/C temperature sensitivity.

IV. Noise Analysis

For sensor resolution to be analytically analyzed, the level and influence on the sensor signal of most dominant noise mechanisms must be evaluated. Modal noise is an inherent feature of the most of the optical fiber sensors with multimode fibers, so it deserves an individual consideration. Also we will analyze how additive noise of any origin affects sensor resolution.

A. Modal Noise Analysis

Despite its importance for smartphone-based optical fiber sensors interrogation, the influence of modal noise on the measured CFBG spectra is usually omitted. The effect of inter-mode interference is well-known and appears to be an obstacle in fiber optic communication systems [35], while it is also harnessed for various measurement applications in singlemode–multimode–singlemode sensors [36]. According to the model derived in [35], speckle visibility at the output of a fiber with length L, group delay dispersion τ irradiated by nonpolarised source with $1/e$ spectral width $\delta\nu$ is given by

$$C = [1 + (\pi\tau\delta\nu L)^2/2]^{-1/4}. \qquad (2)$$

In case of $\delta\nu = 1$ THz, which is equivalent to the above-mentioned spectral resolution $\delta\lambda = 1$ nm, graded-index fiber with length $L = 20$ m and with all nearly equally excited modes, estimation according to eq. (2) yields speckle visibility as low as $C \approx 0.017$, where group delay dispersion was assumed to be 40 ns/km, which is equivalent to 25 MHz · km. The index profile of the used fiber is tailored to provide 500 MHz·km bandwidth at both 850 nm and 1300 nm, however, as follows from the wave theory analysis of graded index fibers (a reader can be referred to a number of textbooks, for example [37]), due to chromatic dispersion of fiber materials, optimal α-profile strongly depends on the wavelength and is a bit less than 2 for 850 nm and 1300 nm windows, while it raises up to 2.15 for 630 nm. At the same time, deviation of fiber profile from the optimal even as small as 0.01 causes around 6 times decrease of the bandwidth [37] and degrades further in case of larger deviations of fiber profile.

On the other hand, the visibility of inter-mode interference signal stipulated by spatial filtering (in our case the slit acts as a spatial filter) is given by [38]

$$V = [(1-\rho)/(\rho \cdot (M+1))]^{1/2}, \tag{3}$$

where relative area $\rho = S_{SF}/S_{beam}$ is the ratio of the aperture through which the light beam is spatially filtered and the initial beam areas and M is the number of propagating modes. Eq. (3) was derived under assumption of unity visibility of speckle pattern, therefore, the spatial filtering corresponds to integration of a pattern with standard deviation equal unity. Due to the speckle visibility decrease described by eq. (2), the resultant interference signal visibility will be C times smaller, as a result, the visibility of parasitic inter-mode interference signal is given by

$$V = [(1-\rho)/(\rho \cdot (M+1))]^{1/2}/[1+(\pi\tau\delta\nu L)^2/2]^{1/4}. \tag{4}$$

In our case of 50 μm optical beam irradiated from the 0.22 NA fiber, travelling about 0.5 mm to the slit causes its broadening to about 135 μm, after which its spatial filtering by 70 μm slit results in relative area $\rho = 0.37$. For the 50 μm graded index fiber with numeric aperture 0.22, there are around $M = 750$ propagating modes for red light, which according to eq. (4) results in parasitic interference signal visibility equal to $V \approx 7.8 \cdot 10^{-4}$. For the measured optical spectrum normalised on the input optical spectrum, V will provide an estimate of modal noise level σ_{MOD}.

Since the modal noises are integrated by the instrument spectral response function (ISRF) of the spectrometer having the width $\delta\lambda$, which is greater than the sampling interval of the spectrum Δ, their impact will not have the form of a white noise, but a low-frequency fluctuations instead. The upper spatial frequency of the modal noise will be inversely proportional to the spectrometer spectral resolution $\delta\lambda$.

It should be noted that the above estimate is approximate and requires precise knowledge of the fiber parameters at the operating wavelength, which are not provided by the manufacturer (obviously, since the fiber is designed for IR light transmission) and obtaining them deliberately requires conducting additional experiments and is out of the scope of the current paper. However, as will be shown in Section V, the estimated level of the modal noise is in a good agreement with the experimental data.

B. Influence of Additive Noise on Sensor Resolution

When the level of additive noise and the analytical equation used for the sensor signal demodulation are known, the measurement resolution can be estimated according to the Cramer-Rao formalism [39], [40], which is widely used for evaluation of the lowest possible variance of the measurement outcome.

The derivation of Cramer-Rao bound for the achievable resolution of BW measurement when the spectrum is fitted by gaussian function given by eq. (1) is performed in Appendix VII. In order to perform the theoretical estimations, the level of the white noise σ_N in the measured CFBG spectra must be evaluated and substituted into eq. (VII.6).

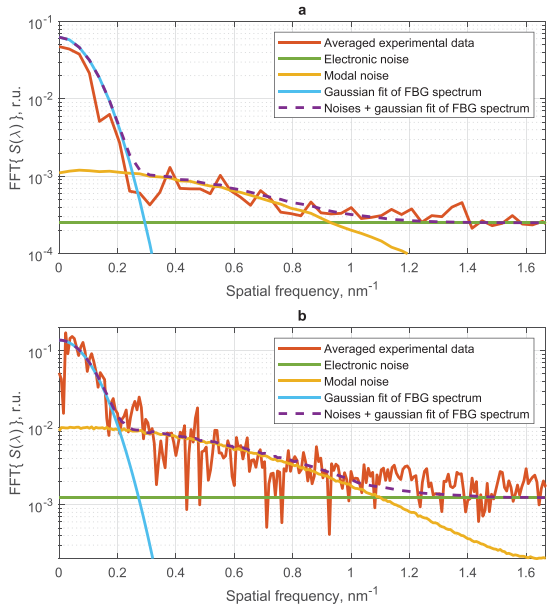

Fig. 5. Comparison of averaged FFT magnitude of the experimentally measured spectra and the estimated noise levels, (a) - SPBS (interrogation rate 0.625 Hz), (b) - commercial spectrometer (interrogation rate 0.5 Hz). The normalisation corresponds to the units of spectral density. Like in spectral and white-light interferometry, the horizontal axis of optical spectrum FFT corresponds to spatial frequency.

The influence of the modal noises on the CFBG readings can also be evaluated with the use of the developed formalism based on the Cramer-Rao relation. An essential assumption made during the derivation of eq. (VII.6) is that the additive noise is white, so its adjacent samples are uncorrelated. As explained above and verified through experiment, which is illustrated in Fig. 5, modal noise is not white, so its samples' values are correlated within the interval of about spectral resolution $\delta\lambda$ width. Therefore, if the measured spectrum is $\delta\lambda/(2\Delta)$ times decimated, the noise samples will become uncorrelated and eq. (VII.6) can be applied. In fact, an identical result will be obtained if the number of points N substituted in eq. (VII.6) is $\delta\lambda/(2\Delta)$ times decreased and the noise is assumed to be white, which is equivalent to the result obtained in [41]. Therefore, in case of a coloured noise, the resolution limit can be estimated from eq. (VII.6) as

$$\sigma_{\lambda_0} \approx 2\frac{\sigma_{MOD}}{A}\sqrt{\frac{aw\delta\lambda}{2\sqrt{\pi}N\Delta}}. \tag{5}$$

Of course, such simplification can be applied only in case of the target signal with relatively small spatial frequencies, which spatial frequency spectrum overlaps with the area of maximal spectral density of the noise, which is true for the considered case of a CFBG.

V. Experimental Validation

In order to validate the proposed smartphone-based CFBG interrogation system concept, we have performed a series of experimental measurements. Strain sensing was chosen as a test example of the CFBG sensor perturbation. The longitudinal

TABLE I
COMPARISON OF THEORETICALLY ESTIMATED AND EXPERIMENTALLY ACHIEVED RESOLUTIONS OF BW MEASUREMENT

A/σ_N	σ_{λ_0}, theory	σ_{λ_0}, experiment
68.6	9.6 pm / 0.053 pixel	11.5 pm / 0.064 pixel

strain from 0 to 2.4 [$m\varepsilon$] with a step of 0.6 [$m\varepsilon$] was applied to the multimode fiber by adding loads from 0 to 2 N with a step of 0.5 N. For each strain value, 10 spectra images were captured with the interrogation rate of 0.625 Hz. The camera settings and the approach of CFBG spectrum processing were the same as those mentioned in Section II and III.

The obtained dependency of the measured BW value on the applied strain is presented in Fig. 4(b). The errorbars indicate standard deviations of the measured BW values at each value of the applied strain. The experimental data was fitted by a linear function, the fit equation is presented in Fig. 4(b) as well. The sensitivity, estimated from the fit turned out to be 0.401 nm/mε or 2.23 pixel/mε. The standard deviation of the BW fitting was below 11.5 pm or 0.064 pixel, which corresponds to standard deviation of strain measurement 29 $\mu\varepsilon$ (for 0.625 Hz interrogation rate); the R^2 for the linear fit approximating the dependency of the CFBG spectral shift on the applied strain is 0.9979.

In order to validate the obtained results we carried out an additional experiment and compared the experimental results with the developed theoretical model based on the Cramer-Rao approach. At first, the change of BW with respect to strain was recorded by commercial Hamamatsu spectrometer as well, the measured CFBG sensitivity comprised 0.399 nm/mε as presented in Fig. 4(b). Therefore, the difference between the results obtained by different measurement devices is around 1%. Also, these sensitivities are in accordance with the previously reported data for FBGs in visible range [42]. The standard deviation of BW measured with Hamamatsu spectrometer was $\sigma_{\lambda_0} = 3.53$ pm for the interrogation rate of 0.5 Hz.

Secondly, we analytically estimated the achievable standard deviation of the measured BW. The standard deviation of the electronic noise was estimated from the residuals between the measured spectra and gaussian fit according to FFT median level algorithm described in [43] and comprised $2.7 \cdot 10^{-4}$ with 0.625 Hz interrogation rate. This value was substituted into eq. (VII.6) with the rest parameters as follows: $N = 161$, $a =$ 14.4 nm (80 pixel), $w = 2.1$ nm (11.7 pixel), $A = 0.019$. Here, averaged values of fitting parameters w and A are reported.

The values of the A/σ_N, which is an analogue of SNR of the measured CFBG spectra, estimated standard deviation of CFBG peak position and average of BW standard deviations at different strain steps are reported in Table I. It should be noted that the Cramer-Rao bound isnt a characteristic of any particular algorithm, but instead gives the fundamental limit of best achievable resolution for a particular measurement task. Therefore, an agreement between theoretical and experimental results of about 20% is good and shows that the utilized signal processing approach is efficient against the noise.

We have also verified the modal noise level estimated by eq. (4) through the analysis of the experimental data obtained by both Hamamatsu and smartphone-based spectrometers. Since the components of measured optical spectrum corresponding to CFBG, modal noise and electronic noise are much easier to be identified when FFT of optical spectra are analyzed, a comparison of measured spectra FFTs with theoretical estimates is shown in Fig. 5(a) for SPBS and (b) for Hamamatsu spectrometer. First of all, FFT of all measured optical spectra were calculated and their magnitudes were averaged in order to obtain smoother and more evident curves. Electronic noises were estimated according to median level of optical spectra FFT, modal noises standard deviations were calculated according to eq. (4), their spectra widths were implied to be equal to inverse spectral resolutions $\delta\lambda$. FFTs of gaussian functions of form (1) representing the CFBG spectrum were also shown. The parameters of optical spectra A, w, levels of electronic and modal noise σ_N, σ_{MOD} and spectral resolutions $\delta\lambda$ obtained by SPBS and Hamamatsu spectrometers are listed in Table II. When the modal noise for Hamamatsu spectrometer was estimated according to eq. (4), it was taken into account that the slit width is 10 μm and the distance between the fiber and the slit was 3 mm. The plotted FFT values were normalised such that they represented the noise spectral density, horizontal axis corresponds to the spatial frequency values of the respective FFT components, similarly to representation of optical spectra FFTs in spectral and white-light interferometry. As can be seen in Fig. 5, both experimentally measured optical spectra are in excellent agreement with the estimations of the considered target and noise components.

TABLE II
COMPARISON OF SPECTROMETERS PARAMETERS AND MEASUREMENT RESULTS

Parameter	Notation	SPBS	Hamamatsu	Unit
Spectral response range	–	410-680	200-800	nm
Wavelength scale	Δ	0.18	0.35 (at 634 nm)	nm/ pixel
Spectral resolution (FWHM of ISRF)	$\delta\lambda$	1	1	nm
Slit width	–	70	10	μm
Wavelength temperature dependence	–	0.024	0.04	nm/C
Modal noise	σ_{MOD}	$7.8 \cdot 10^{-4}$	$6.1 \cdot 10^{-3}$	r.u.
Additive noise	σ_N	$3.41 \cdot 10^{-4}$	$1.56 \cdot 10^{-3}$	r.u./ $\sqrt{\text{Hz}}$
CFBG peak amplitude, gaussian fit	A	0.019	0.18	r.u.
Half width at $1/\sqrt{e}$ of maximum, gaussian fit	w	2.1	2.25	nm
FWHM of measured CFBG spectrum	–	6	6	nm
Measurement resolution (standard deviation of measured BW)	σ_{λ_0}	14.5 0.081	5 0.014	pm/ $\sqrt{Hz}$ pixel/ $\sqrt{Hz}$

As supported by the analysis described above, the assumptions made during the derivation of the modal noise properties are correct, so the BW uncertainty caused by the modal noise can be estimated according to eq. (5) to be around $\sigma_{\lambda_0} \approx 45$ pm.

However, such large variation of the measured BW values can be produced only if the modal noise realisations in different spectra are completely uncorrelated, which requires a significant perturbation of a large section of the feeding MM fiber to take place. However, we believe that the detailed consideration of the modal noise influence on smartphone-interrogated sensors requires a separate investigation and falls out of the scope of the current paper.

VI. Discussion and Conclusion

The smartphone-based interrogation of a fiber Bragg grating sensor was, to the best of our knowledge, demonstrated for the first time. The interrogated CFBG was inscribed in a standard graded-index multimode fiber. Interrogation setup consists of low cost and readily available components. The proof-of-concept experiment was performed by sensing strain applied to the CFBG. The developed prototype of a smartphone-based CFBG sensing system demonstrates picometer-level Bragg wavelength and micro-strain-level strain measurement resolution and excellent linearity. The obtained results were validated with the use of a commercial spectrometer and by theoretical analysis. Also, to the best of our knowledge, the work contains the first analysis of the modal noise effects in smartphone-based interrogation systems for optical fiber sensors with a spectral read-out.

The goal of the present work, however, is not to make a replacement of conventional FBG interrogators operating at telecommunication windows. It is obvious that the devices that are tailored for the FBG interrogation will outperform those based on a general-purpose platforms such as smartphones. However, we believe that this work, along with the other studies on smartphone-based interrogation of optical fiber sensors will pave the way for ultra-low cost, wide-spread and portable sensing systems that will unite the advantages offered by the optical fiber sensors and the smartphones. Moreover, even this pilot study was able to clearly demonstrate the feasibility of further research on smartphone-based interrogation of OFS, including those based on various gratings, as well as to probe a prominent way to implement a smartphone-based fiber grating interrogation and to identify the obstacles that are yet to be overcame.

We would also like to emphasize that the achieved characteristics of the developed smartphone-based spectrometer are similar and some even superior to those of a commercial Hamamatsu spectrometer, used in this work as a reference. The Bragg wavelength measurement resolution achieved with Hamamatsu spectrometer was better, however, the measurement resolution of a smartphone-based spectrometer can be substantially improved when a fiber grating better suited for the task is interrogated. The comparison of spectrometers' characteristics and Bragg wavelength measurement resolutions is presented in Table II.

Further work should be directed towards performance improvement of the smartphone-based spectrometer, application of the developed technique for the interrogation of FBG arrays and other fiber optic sensors, further analysis and suppression of modal noise mechanisms. Moreover, as follows from the presented analysis, the properties of the fibers and gratings used for the sensing elements of the smartphone-interrogated sensors must be selected very carefully, additional evaluation of their characteristics at visible wavelengths would also advance the field. In case of a smartphone-based spectral interrogation of MMF sensors, accurate tailoring of their characteristics for particular applications is also a key to achieving superior performance.

Appendix A

Cramer-Rao Lower Bound for BW Resolution Cramer-Rao lower bound for CFBG BW λ_0 parameter estimation resolution can be found as [40]

$$\sigma_{\lambda_0} = \left[\frac{1}{\sigma_N} \sqrt{\sum_{i=1}^{N} \left(\frac{\partial S_i}{\partial \lambda_0} \right)^2} \right]^{-1}, \tag{A.1}$$

where σ_{λ_0} – standard deviation of λ_0, S_i – samples of the measured CFBG spectrum, N – number of spectral points, σ_N – standard deviation of additive noise, which is assumed to be white and gaussian.

In this work we approximate the measured CFBG spectrum by a gaussian function as in eq. (1). The sum in equation (A.1) can than be rewritten in the following form

$$\sum_{i=1}^{N} \left(\frac{\partial S_i}{\partial \lambda_0} \right)^2 = \sum_{i=1}^{N} \frac{A^2}{w^4} \left(\lambda_i - \lambda_0 \right)^2 e^{\left(-\frac{(\lambda_i - \lambda_0)^2}{w^2} \right)}. \tag{A.2}$$

We substitute $\lambda_i - \lambda_0$ for a new variable λ_i'

$$\sum_{i=1}^{N} \left(\frac{\partial S_i}{\partial \lambda_0} \right)^2 \approx \sum_{i=-N/2}^{N/2} \frac{A^2}{w^4} {\lambda'}_i^2 e^{2\left(-\frac{\lambda_i'^2}{w^2} \right)}. \tag{A.3}$$

In case of relatively large number N of summation terms, there is an equivalence between the last sum and a definite integral

$$\sum_{i=-N/2}^{N/2} \left(\frac{\partial S_i}{\partial \lambda_0} \right)^2 \approx \frac{N}{2a} \int_{-a}^{a} \frac{A^2}{w^4} \lambda^2 e^{\left(-\frac{\lambda^2}{w^2} \right)} d\lambda, \tag{A.4}$$

where a is the width of the spectral interval containing all N points that are approximated. The integral in (A.4) can be rewritten in the next form

$$\sum_{i=-N/2}^{N/2} \left(\frac{\partial S_i}{\partial \lambda_0} \right)^2 \approx \frac{N\sqrt{\pi} A^2}{4aw} \operatorname{erf}\left(\frac{a}{w} \right) - \frac{N A^2}{2\, w^2} e^{\left(-\frac{a^2}{w^2} \right)}, \tag{A.5}$$

where erf is the error function. In case of rather large $a > 3\, w$ we can simplify the first term and neglect the second term. Therefore, the Cramer-Rao lower bound for the Bragg wavelength standard deviation can be written in the following form

$$\sigma_{\lambda_0} \approx 2 \frac{\sigma_N}{A} \sqrt{\frac{aw}{\sqrt{\pi} N}}, \tag{A.6}$$

ACKNOWLEDGMENT

The authors would like to thank Alexey I. Gribaev for providing the CFBG used in the experiment, Ekaterina A. Semina for the fruitful discussions concerning the narrative of the manuscript and Oleg I. Kotov for the helpful comments on the mechanisms of the modal noise.

REFERENCES

[1] A. Aitkulov and D. Tosi, "Optical fiber sensor based on plastic optical fiber and smartphone for measurement of the breathing rate," *IEEE Sensors J.*, vol. 19, no. 9, pp. 3282–3287, May 2019.

[2] T. Konishi and Y. Yamasaki, "Compact and cost-effective multi-channel optical spectrometer for fine FBG sensing in IoT technology," in *Proc. SPIE*, vol. 10551, 2018, Art. no. 105510L.

[3] M. Pisco *et al.*, "Opto-mechanical lab-on-fibre seismic sensors detected the Norcia earthquake," *Scientific Rep.*, vol. 8, no. 1, 2018, Art. no. 6680.

[4] T. Yamate, G. Fujisawa, and T. Ikegami, "Optical sensors for the exploration of oil and gas," *J. Lightw. Technol.*, vol. 35, no. 16, pp. 3538–3545, 2017.

[5] T. Kasai *et al.*, "Fiber-optic simultaneous distributed monitoring of strain and temperature for an aircraft wing during flight," *Appl. Opt.*, vol. 57, no. 36, pp. 10 458–10 465, 2018.

[6] K. O. Hill and G. Meltz, "Fiber bragg grating technology fundamentals and overview," *J. Lightw. Technol.*, vol. 15, no. 8, pp. 1263–1276, 1997.

[7] T. Erdogan, "Fiber grating spectra," *J. Lightw. Technol.*, vol. 15, no. 8, pp. 1277–1294, 1997.

[8] D. Tosi, "Review of chirped fiber Bragg grating (CFBG) fiber-optic sensors and their applications," *Sensors (Switzerland)*, vol. 18, no. 7, 2018, Art. no. 2147.

[9] Q. Liu, Y. Liu, H. Yuan, F. Wang, and W. Peng, "A smartphone-based red-green dual color fiber optic surface plasmon resonance sensor," *IEEE Photon. Technol. Lett.*, vol. 30, no. 10, pp. 927–930, 2018.

[10] T. C. Wilkes, A. J. S. McGonigle, J. R. Willmott, T. D. Pering, and J. M. Cook, "Low-cost 3D printed 1 nm resolution smartphone sensor-based spectrometer: Instrument design and application in ultraviolet spectroscopy," *Opt. Lett.*, vol. 42, no. 21, 2017, Art. no. 4323.

[11] Z. Geng, X. Zhang, Z. Fan, X. Lv, Y. Su, and H. Chen, "Recent progress in optical biosensors based on smartphone platforms," *Sensors (Switzerland)*, vol. 17, no. 11, pp. 1–19, 2017.

[12] L. Kong *et al.*, "A novel smartphone-based CD-spectrometer for high sensitive and cost-effective colorimetric detection of ascorbic acid," *Analytica Chimica Acta*, vol. 1093, pp. 150–159, 2020.

[13] K. Bremer and B. Roth, "Fibre optic surface plasmon resonance sensor system designed for smartphones," *Opt. Express*, vol. 23, no. 13, 2015, Art. no. 17179.

[14] M. A. Hossain, J. Canning, K. Cook, and A. Jamalipour, "Optical fiber smartphone spectrometer," *Opt. Lett.*, vol. 41, no. 10, 2016, Art. no. 2237.

[15] L. Lu *et al.*, "A portable optical fiber SPR temperature sensor based on a smart-phone," *Opt. Express*, vol. 27, no. 18, 2019, Art. no. 25420.

[16] T. Pan, W. Cao, and M. Wang, "TiO_2 thin film temperature sensor monitored by smartphone," *Opt. Fiber Technol.*, vol. 45, pp. 359–362, 2018.

[17] T. Liu, W. Wang, H. Ding, Z. Liu, S. Zhang, and D. Yi, "Development of a handheld dual-channel optical fiber fluorescence sensor based on a smartphone," *Appl. Opt.*, vol. 59, no. 3, p. 601, 2020.

[18] Y. Chen *et al.*, "A portable smartphone-based vector-magnetometer illuminated and imaged via a side-polished-fiber functionalized with magnetic fluid," *IEEE Sensors J.*, vol. 20, no. 3, pp. 1283–1289, Feb. 2020.

[19] H. J. Kalinowski, G. Capote Mastrapa, G. G. Guimarães, P. L. Inácio, and V. Oliveira, "Fibre bragg gratings in the visible: Towards low-cost detection," in *Proc. SPIE*, vol. 10680, 2018, p. 106800N.

[20] A. W. Snyder and C. Pask, "Incoherent illumination of an optical fiber," *J. Opt. Soc. Amer.*, vol. 63, no. 7, pp. 806–812, 1973.

[21] M. Salem and G. P. Agrawal, "Effects of coherence and polarization on the coupling of stochastic electromagnetic beams into optical fibers," *J. Opt. Soc. America A*, vol. 26, no. 11, pp. 2452–2458, 2009.

[22] M. Salem and G. P. Agrawal, "Effects of coherence and polarization on the coupling of stochastic electromagnetic beams into optical fibers: Errata," *J. Opt. Soc. Amer. A*, vol. 28, no. 3, pp. 307–307, 2011.

[23] J. F. Kuhne, A. M. Rocha, V. De Oliveira, H. J. Kalinowski, and R. C. Kamikawachi, "Experimental and numerical study on refractive index sensors based on fibre Bragg gratings inscribed in multimode fibre," *Meas. Sci. Technol.*, vol. 29, no. 2, 2018, Art. no. 025102.

[24] C. Broadway, R. Min, A. G. Leal-Junior, C. Marques, and C. Caucheteur, "Toward commercial polymer fiber bragg grating sensors: Review and applications," *J. Lightw. Technol.*, vol. 37, no. 11, pp. 2605–2615, 2019.

[25] A. Theodosiou and K. Kalli, "Recent trends and advances of fibre Bragg grating sensors in CYTOP polymer optical fibres," *Opt. Fiber Technol.*, vol. 54, 2020, Art. no. 102079.

[26] A. I. Gribaev, I. V. Pavlishin, A. M. Stam, R. F. Idrisov, S. V. Varzhel, and K. A. Konnov, "Laboratory setup for fiber Bragg gratings inscription based on Talbot interferometer," *Opt. Quantum Electron.*, vol. 48, no. 12, 2016.

[27] M. J. Schmid and M. S. Müller, "Measuring bragg gratings in multimode optical fibers," *Opt. Express*, vol. 23, no. 6, 2015, Art. no. 8087.

[28] A. Theodosiou, X. Hu, C. Caucheteur, and K. Kalli, "Bragg gratings and Fabry–Perot cavities in low-loss multimode CYTOP polymer fiber," *IEEE Photon. Technol. Lett.*, vol. 30, no. 9, pp. 857–860, 2018.

[29] N. V. Tkachenko, "Chapter 2 - optics and optical devices," in *Opt. Spectroscopy*, N. V. Tkachenko, Ed. Amsterdam: Elsevier Science, 2006, pp. 15–38.

[30] L. Rodriguez-Cobo, M. Lomer, and J. M. Lopez-Higuera, "Fiber specklegram-multiplexed sensor," *J. Lightw. Technol.*, vol. 33, no. 12, pp. 2591–2597, 2015.

[31] I. Chapalo, A. Petrov, D. Bozhko, M. A. Bisyarin, and O. I. Kotov, "Averaging methods for a multimode fiber interferometer: Experimental and interpretation," *J. Lightw. Technol.*, pp. 1–1, 2020.

[32] A. Theodosiou, A. Ioannou, and K. Kalli, "All-in-fiber cladding interferometric and bragg grating components made via plane-by-plane femtosecond laser inscription," *J. Lightw. Technol.*, vol. 37, no. 18, pp. 4864–4871, 2019.

[33] V. Mizragi and J. E. Sipe, "Optical properties of photosensitive fiber phase gratings," *J. Lightw. Technol.*, vol. 11, no. 10, pp. 1513–1517, 1993.

[34] S. Kumar, B. Amrutur, and S. Asokan, "Evaluation of fiber Bragg grating sensor interrogation using InGaAs linear detector arrays and Gaussian approximation on embedded hardware," *Rev. Scientific Instruments*, vol. 89, no. 2, 2018, Art. no. 025102.

[35] R. Dandliker, A. Bertholds, and F. Maystre, "How modal noise in multimode fibers depends on source spectrum and fiber dispersion," *J. Lightw. Technol.*, vol. 3, no. 1, pp. 7–12, 1985.

[36] K. Wang *et al.*, "Advances in optical fiber sensors based on multimode interference (MMI): A review," *IEEE Sensors J.*, pp. 1–1, 2020.

[37] K. Okamoto, "3.7 – wave theory of graded-index fibers," in *Proc. Fundam. Opt. Waveguides*, 2nd ed. Amsterdam: Elsevier, 2006, pp. 103–116.

[38] J. W. Goodman and E. G. Rawson, "Statistics of modal noise in fibers: A case of constrained speckle," *Opt. Lett.*, vol. 6, no. 7, p. 324, 1981.

[39] D. Slepian, "Estimation of signal parameters in the presence of noise," *Trans. IRE Prof. Group Inf. Theory*, vol. 3, no. 3, pp. 68–89, 1954.

[40] D. Zachariah and P. Stoica, "Cramer–Rao bound analog of bayes' rule [Lecture notes]," *IEEE Signal Process. Mag.*, vol. 32, no. 2, pp. 164–168, 2015.

[41] A. A. Ushakov, Nikolai A. Markvart and L. B. Liokumovich, "Pulse wave velocity measurement with multiplexed fiber optic fabry-perot interferometric sensors," *IEEE Sensors J.*, vol. 20, no. 19, pp. 11 302–11 312, 2020.

[42] P. L. Inácio, I. da Silva Vasco Sualehe, I. Chiamenti, V. de Oliveira, and H. J. Kalinowski, "Characterization of femtosecond-inscribed fiber Bragg gratings in the visible spectral region," *Appl. Opt.*, vol. 56, no. 3, p. 510, 2017.

[43] N. A. Ushakov and L. B. Liokumovich, "Signal processing approach for spectral interferometry immune to $\lambda/2$ Errors," *IEEE Photon. Technol. Lett.*, vol. 31, no. 18, pp. 1483–1486, Sep. 2019.